Fusion Engineering and Design 200 (2024) 114240

Contents lists available at ScienceDirect

Fusion Engineering and Design

journal homepage: www.elsevier.com/locate/fusengdes

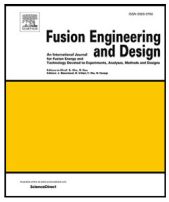

Hypothetical porous medium concept as a virtual swirl tape: A novel modelling technique towards efficient CFD simulation of swirl tape cooling pipe

A. Quartararo [a,*], S. Basile [a], G. Bongiovì [a], R. Burlon [a], F.M. Castrovinci [a], I. Catanzaro [a], P. Chiovaro [a], P.A. Di Maio [a], G. Mazzone [b], E. Vallone [a], J.H. You [c]

[a] Department of Engineering, University of Palermo, Viale delle Scienze, Ed. 6, 90128 Palermo, Italy
[b] Department of Fusion and Technology for Nuclear Safety and Security, ENEA C.R. Frascati, via E. Fermi 45, 00044 Frascati (Roma), Italy
[c] Max Planck Institute of Plasma Physics (E2M), Boltzmann Str.2, 85748 Garching, Germany

ARTICLE INFO

Keywords:
DEMO
Divertor
PFC
Thermofluid-dynamics
CFD analysis
Optimization

ABSTRACT

The EU-DEMO divertor target cooling circuit is equipped with Swirl Tape (ST) inserts to improve its thermo-hydraulic performance in terms of heat transfer coefficient and critical heat flux. Due to the presence of the STs, accurate 3D CFD-based thermofluid-dynamic assessments of the divertor targets cooling circuit require a high computational cost and a laborious pre-processing modelling effort. To this end, a cost-efficient CFD simulation technique based on an equivalent porous medium concept, namely the Virtual Swirl Tape (VST) approach, has been developed. In this work, the mathematical formulation of different VSTs models is presented, and the porous media calibration procedure and validation are shown. This technique enables the reduction of computational costs by decreasing the number of volumes required for a single Plasma-Facing Unit (PFU) assembly cooling channel by a factor of 10, while lowering the calculation time by ≈86%. The results obtained show that it is possible to correctly reproduce the friction factor profile and pressure drop of a PFU assembly cooling channel, this latter with errors within 10% considering a wide range of coolant inlet velocities. Some limitations have been observed concerning the VST thermal performance, which is still unsatisfactory and requires further development. The VST approach has been studied using the commercial CFD code ANSYS CFX, coupled with a multi-objective optimization algorithm available in the ANSYS Direct Optimization tool.

1. Introduction

The divertor is the key in-vessel component of fusion reactors devoted to power handling and impurity removal. Its importance is highlighted by the European Research Roadmap to the Realization of Fusion Energy [1], which defines reliable power exhausting as one of the most critical missions to be accomplished.

The divertor must be capable of withstanding the huge heat and particle fluxes foreseen for a nuclear fusion device and, therefore, power plant scale reactors, such as the EU-DEMO, require proper cooling and must rely on the adoption of heat transfer enhancement techniques to improve the performance of the cooling circuit of the Vertical Targets (VTs), the most critical components from a thermal viewpoint. In the case of the EU-DEMO, ST inserts are adopted inside the VTs cooling channels [2], similarly to other tokamaks machines [3–6], to improve both the heat transfer coefficient and the Critical Heat Flux (CHF) margin.

An accurate thermo-hydraulic assessment of the VTs cooling circuit equipped with STs generally requires the adoption of 3D Computational Fluid-Dynamic (CFD)-based calculations. To correctly simulate the STs, a laborious pre-processing modelling effort and a high computational cost are necessary, due to the quite high volume density needed to obtain grid-independent results, as discussed in [7]. Moreover, the computational cost required may be excessively high for complex simulations, such as the one reported in [8]. Therefore, it is desirable to define cost-efficient simulation techniques aimed at significantly reducing the computational cost required to simulate the ST-equipped cooling channels while maintaining a good accuracy of the results. A novel simulation technique based on an equivalent porous medium concept, namely the Virtual Swirl Tape (VST), has been developed.

A numerical approach based on the finite volume method has been followed, adopting the well-established ANSYS CFX 2021 commercial CFD code [9] coupled with the ANSYS Direct Optimization tool [10].

* Corresponding author.
E-mail address: andrea.quartararo@unipa.it (A. Quartararo).

https://doi.org/10.1016/j.fusengdes.2024.114240
Received 6 October 2023; Received in revised form 26 December 2023; Accepted 8 February 2024
Available online 13 February 2024

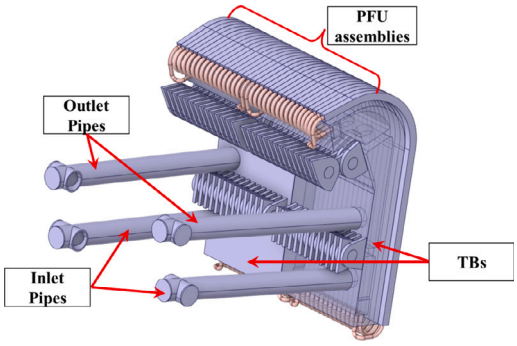

Fig. 1. DEMO divertor IVT (2021 design).

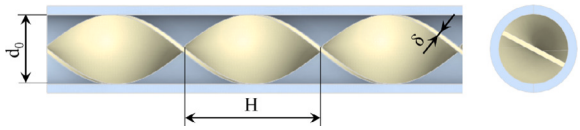

Fig. 2. Section of the ST-equipped cooling channel with an indication of its geometrical features.

2. Outline of plasma-facing unit cooling channels

The design currently considered for the cooling of the EU DEMO divertor VTs foresees each target composed of a couple of Target Bodys (TBs), box-like structures on which the Plasma Facing Unit (PFU) assemblies are mounted. The TBs act as distributors and collectors for the coolant. In particular, 34 PFU assemblies are envisioned for the Inner VT (IVT) and 46 for the Outer VT (OVT). The IVT of the DEMO divertor is depicted in Fig. 1, showing the TBs and the PFU assemblies.

The details of the PFU assemblies and of the geometry of the single PFUs are thoroughly described in [2]. Regarding the cooling of these components, each PFU assembly is cooled by a single CuCrZr pipe, equipped in its straight part with a ST. The main geometrical parameters of these pipes are the internal diameter d_0, the ST thickness δ, and the ST pitch H, respectively equal to 12, 0.8, and 24 mm. The length of the assemblies and the geometry of the bends of the cooling channel depend instead on whether the IVT or the OVT are considered. A section of the straight part of one of the pipes is depicted in Fig. 2.

The VT cooling circuit should be able to provide adequate cooling to the PFU assemblies and TBs under normal and off-normal operating conditions. In particular, the design of this cooling circuit is dictated by the need to have an adequate margin against CHF under slow-transient loads (characterized by peak heat fluxes of ≈ 20 MW/m^2 and a duration in the order of 10s of seconds, long enough to reach the thermal equilibrium of the target structures), while maintaining a reasonable pressure drop. The CHF margin calculation is usually done by adopting proper correlations, as the one reported in [3], and it requires the knowledge of the coolant bulk temperature, the mass flow rate, and the local pressure value. While the first can be easily estimated with energy conservation reasonings, local pressure and mass flow rate are both related to the prediction of pressure drop inside the PFU cooling channels connected in parallel. Therefore, a correct estimation of the pressure distribution inside this cooling circuit is sufficient to provide most of the information useful for assessing the circuit's performance.

3. Detailed simulations of a PFU cooling channel

Detailed isothermal 3D-CFD simulations of an entire OVT PFU assembly cooling channel (drawn from the 2021 EU-DEMO divertor design [11], characterized by a total cooling channel length of $\approx$ 1400 mm and a ST length of 660 mm) have been carried out with the aim of comparing the results in terms of pressure drop with the correlations available in literature. The occurrence of deviations from these correlations related to localized fluid-dynamic phenomena has been assessed.

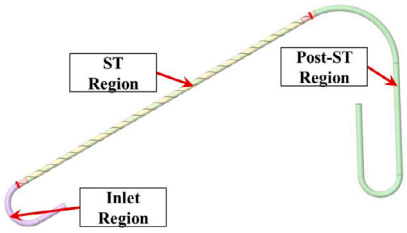

Fig. 3. PFU cooling channel computational domain.

Table 1
Summary of assumptions, models and BCs for the PFU cooling channel calculations.

Analysis type	Steady-state isothermal
Material library	Water (constant properties)
Reference temperature	133 °C
Turbulence model	k-ω SST
Boundary layer modelling	Automatic wall function
Pipe/ST roughness	1 μm/0.5 μm [3]
Coolant inlet velocity	6 to 16 m/s
Outlet total pressure	45 bar

Table 2
PFU cooling channel analysis mesh parameters.

Mesh parameter	Value
Mesh type	Hybrid Hexa - Tetra
Nodes	$4.86 \cdot 10^6$
Elements	$5.06 \cdot 10^6$
Inflation layers number	12
First cell height [μm]	20
Target element size [mm]	0.59
Surface with $y^+ > 100$ [%]	0

The computational domain considered for the analyses is the one depicted in Fig. 3, which has been simulated assuming the coolant operative conditions, models, Boundary Conditions (BCs), and assumptions summarized in Table 1. The selected values of coolant average temperature and pressure have been chosen based on the baseline divertor operating conditions [12], while a broad range of coolant velocity has been considered, in order to obtain results applicable both to the baseline VT cooling circuit [12] and the single-circuit 2021 design [8]. Moreover, the small gap between the tape and the cooling channel has been neglected, as it is supposed to be small enough ($\approx$ 0.1 mm) not to significantly affect the coolant flow field. Furthermore, the k-ω SST turbulence model has been selected, being the one usually employed to perform the CFD simulations of the divertor cooling circuit [8] and since it provided a good agreement with experimental results in [7].

The mesh features selected for the CFD simulation are summarized in Table 2. In particular, a bulk mesh size of 0.59 mm has been chosen, based on the outcomes of [7], in order to obtain fairly mesh-independent results. Some details of the mesh set up for the PFU analysis are shown in Fig. 4.

As the aim of the analysis is to evaluate the pressure losses within the PFU cooling channel, the attention has been focused on the Fanning friction factor f, defined according to Eq. (1).

$$f = \frac{\Delta p}{L} \frac{d_0}{2\rho u_0^2} \tag{1}$$

With reference to the equation above, $\Delta p/L$ is the total pressure drop per unit length of the channel, ρ is the fluid density, and u_0 is the empty-channel axial velocity, calculated as $u_0 = 4G/(\rho\pi d_0^2)$, where G

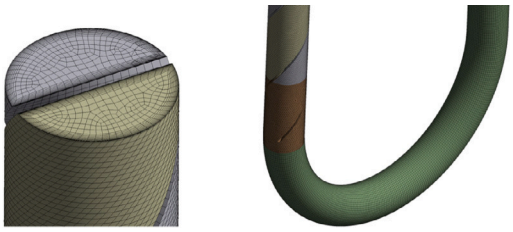

Fig. 4. Detail of the mesh adopted for the PFU cooling channel CFD analysis.

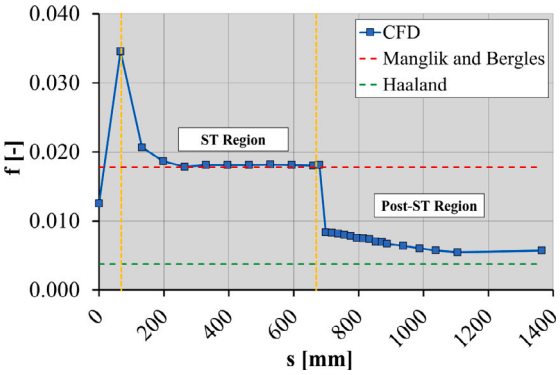

Fig. 5. Local Fanning friction factor along the PFU cooling channel curvilinear abscissa.

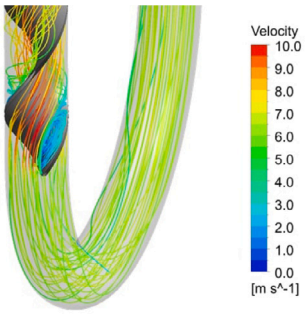

Fig. 6. Details of the flow field at the entrance of the ST region.

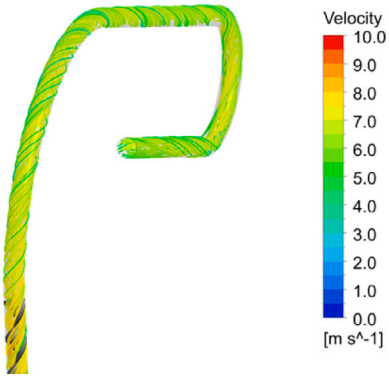

Fig. 7. Persistence of the swirling motion in the post-ST region.

is the mass flow rate. By adopting this formulation, the coolant velocity is evaluated not considering the presence of the ST, following the approach detailed in [13]. To derive the friction factor from the CFD calculation, 29 monitoring planes perpendicular to the channel axis have been considered from the inlet to the outlet of the pipe. For a given monitoring plane i, the friction factor has been calculated according to Eq. (1), where the term $\Delta p/L$ has been replaced by $\left(p_i - p_{i-1}\right)/l$, where p_i and p_{i-1} are the area-averaged static pressure calculated at the plane i and $i-1$, and l is the distance between the planes.

The results obtained in terms of local Fanning friction factor along s, the curvilinear abscissa of the pipe axial line, are shown in Fig. 5 (the origin of the abscissa corresponds to the entrance of the ST region) for the case of coolant inlet velocity of 6 m/s.

The figure also reports the comparison with Manglik and Bergles correlation valid for ST-equipped pipes [13], given in Eq. (2), and Haaland correlation [14] valid for straight empty pipes, detailed in Eq. (3).

$$f = 0.0791\,\mathrm{Re}_0^{-0.25}\left(\frac{\pi + 2 - \left(2\delta/d_0\right)}{\pi - \left(4\delta/d_0\right)}\right)^{1.25} \cdot \left(\frac{\pi}{\pi - \left(4\delta/d_0\right)}\right)^{1.75}\left(1 + 2.752\left(\frac{d_0}{H}\right)^{1.29}\right) \tag{2}$$

$$\frac{1}{\sqrt{f}} = -3.6\log\left(\frac{6.9}{\mathrm{Re}_0} + \left(\frac{\sigma}{3.7d_0}\right)^{1.11}\right) \tag{3}$$

With reference to Eqs. (2) and (3), Re_0 is the Reynolds number calculated for the empty pipe, while σ is the sand-grain equivalent surface roughness.

As can be noted from Fig. 5, there are two main deviations from the relevant correlations: an initial peak, corresponding to the inlet section of the ST region, and a higher friction factor value in the post-ST region, decaying along the curvilinear abscissa. The results obtained for all the other coolant velocities are qualitatively similar, showing the same features.

Regarding the initial peak, it is related to the presence of strong flow separation at the entrance of the ST region, as clearly visible in Fig. 6. The separation occurs only on one side of the ST, far from the axis of the cooling channel, mainly promoted by the local unfavourable curvature of the ST. Even if it is localized on a length scale of $\approx H$, it is responsible for almost 7% of the overall pressure drop inside the entire PFU cooling channel.

Concerning the second effect, i.e. a higher pressure drop in the post-ST region, it is instead due to the persistence of the swirling motion in the region downstream of the ST, as clearly visible in Fig. 7.

As it may be observed, the swirling motion decays moving towards the outlet, resulting in a straightening of the fluid flow inside the pipe due to the occurrence of viscous forces, and is almost completely lost after the sharp bend in the final part of the PFU channel. The magnitude of this second effect is estimated to account for $\approx$ 2% of the total pressure drop inside the entire PFU channel. However, this effect may become more relevant if, for example, shorter STs are equipped, or if the shape of the post-ST region of the cooling channel is different.

Summing up these two effects, they result in a $\approx$ 10% of the overall pressure drop inside the PFU cooling channel, and thus they must be taken into account to avoid an excessive underestimation of the pressure drop.

The same qualitative results can also be obtained for other PFU cooling channel geometries such as the IVT.

4. The virtual swirl tape approach

The development of a numerical model relying on the adoption of porous media domains to reproduce the effect of the ST in terms of pressure drop has been pursued, taking into account the deviations highlighted in the previous section.

This novel approach, called VST, has been developed focussing on two different modelling techniques, namely the Isotropic VST (IVST) and Orthotropic VST (OVST), detailed in the following.

Employing the VST model significantly eases the pre-processing effort, as geometry cleaning and mesh generation are greatly simplified, and reduces the computational cost required to perform complex

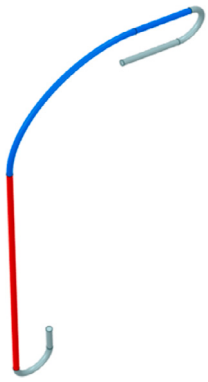

Fig. 8. Porous regions adopted in the IVST approach.

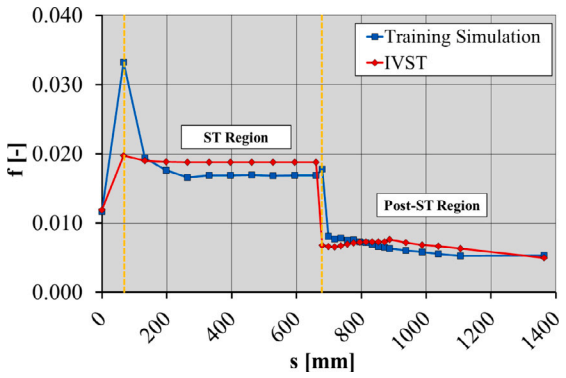

Fig. 9. Comparison of local Fanning friction factor along the PFU cooling channel curvilinear abscissa between training simulation and IVST approach.

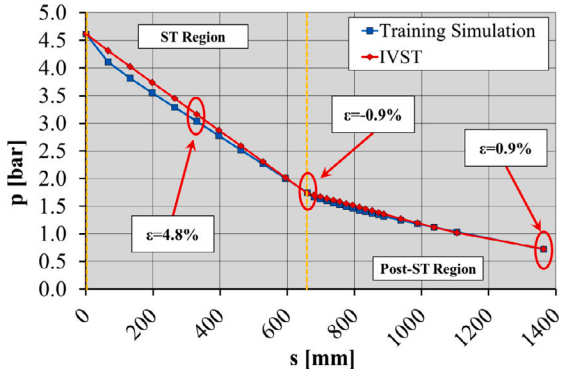

Fig. 10. Comparison of pressure evolution along the PFU cooling channel curvilinear abscissa between training simulation and IVST approach.

simulations with ST inserts. In particular, it is possible to reduce the number of cells required to simulate these components because of the absence of the tape itself (accompanied by a reduction in the number of boundary layers cells and the possibility of avoiding local refinements in the terminal parts of the ST), together with the possibility to select arbitrarily coarse elements for the porous media, as mesh-related errors can be compensated by an optimal selection of the porous media coefficients.

4.1. The isotropic virtual swirl tape approach

The IVST approach is based on the adoption of two distinct porous regions, one aimed at reproducing the pressure drop inside the ST (accounting for both the initial flow separation-induced peak and the fully-developed swirling motion inside the ST-equipped pipe), and the other simulating the additional losses encountered inside the post-ST region, due to the swirling motion decay already discussed in Section 3. The choice of employing precisely two porous media is a compromise between model complexity and accuracy of the results. These two porous regions are shown respectively in red and blue in Fig. 8, where it is possible to note how the blue porous region is extended up to the upper straight part of the PFU cooling channel, coherently with the results discussed in the previous section.

Each one of the two regions is simulated taking into account a properly calibrated isotropic momentum sink term $\underline{S}$ in the Navier–Stokes equations, given in Eq. (4), where K_{loss} is a loss coefficient, $\underline{u}$ is the local velocity vector, and $\|\cdot\|$ is the norm operator.

$$\underline{S} = -K_{loss}\frac{\rho}{2}\|\underline{u}\|\,\underline{u} \tag{4}$$

According to this equation, the force per unit volume acting on the fluid $\underline{S}$ is oriented along the same direction as the velocity vector $\underline{u}$ due to the isotropy of the loss coefficient, here reported as a scalar quantity for simplicity.

The K_{loss} coefficients relevant to the two porous regions can be determined starting from detailed CFD simulations encompassing the ST, such as those presented in Section 3. In particular, one simulation, referred to in the following as *training simulation*, is performed considering the relevant coolant operating conditions and mass flow rate. This simulation is carried out to calculate the overall pressure drop inside the entire PFU cooling channel and the pressure drop occurring uniquely in the ST region. Therefore, the K_{loss} coefficients of the porous media are obtained by means of dedicated optimization studies, performed by adopting the ANSYS Direct Optimization tool coupled with ANSYS CFX. In particular, a Multi-Objective Genetic Algorithm (MOGA) optimizer has been selected. These studies allow selecting a couple of K_{loss} coefficients for the two porous regions such that the overall pressure drop and the pressure drop of the ST region calculated with the IVST reproduce with the smallest error those of the training simulation.

The IVST calculations have been performed considering a mesh bulk size of 1.3 mm, generated with the same layer parameters reported in Table 2, thus obtaining a mesh made up of $5.8 \cdot 10^5$ elements and $5.6 \cdot 10^5$ nodes. Compared to the training simulation, the overall number of cells and nodes is reduced by a factor of 10. Additionally, the calculation time required to obtain convergence ($\approx$ 100 iterations) has been reduced from 46 to 7 min on an 18-core Intel i9-9980XE processor @3.00 GHz.

The calibration procedure has been performed considering a reference coolant velocity of 12 m/s for the training simulation. The IVST optimization analyses have been performed with the same coolant velocity, while all the other assumptions, models, and BCs are in line with those of Table 1. The optimization procedure required $\approx$ 200 iterations to converge.

The comparison of the local Fanning friction factor along the PFU cooling channel curvilinear abscissa is provided in Fig. 9, while the pressure evolution along the cooling channel is depicted in Fig. 10. An indication of the relative error between the IVST and the training simulation in terms of static pressure at three different sections of the cooling channel is moreover provided in the latter figure.

Fig. 9 shows that the initial peak is significantly underestimated by the IVST approach and its effect on pressure drop is compensated by a constant and increased loss coefficient along the entire ST region. It results in a pressure value at the outlet of the ST region close to the one of the training simulation. The post ST region instead presents some fluctuations in the Fanning friction factor profile, and the porous medium is not able to compensate for the lack of swirling flow, thus resulting in a lower pressure drop. The overall behaviour of this approach is however acceptable, and the Δp deviates by a small

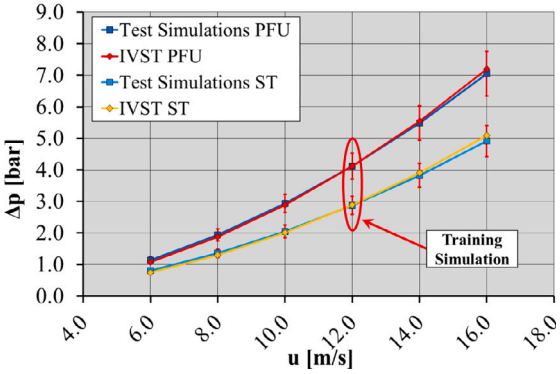

Fig. 11. Comparison of pressure drop prediction between test simulations and IVST approach.

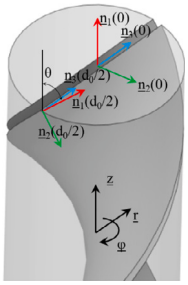

Fig. 12. Main directions adopted for the OVST modelling.

amount from the desired target value. The relative errors reported in Fig. 10 are calculated at the ST mid-section, where the strike point is supposed to be located, at the outlet of the ST, and at the outlet of the entire cooling channel. The maximum deviation is obtained at the ST mid-section and it is below 5%, while the error in the prediction of the total pressure drop is below 0.1%.

An additional set of analyses has been performed by changing the inlet velocity ranging from 6 to 16 m/s and comparing the results with those obtained with the simulations of Section 3 (these latter are referred to in the following as *test simulations*) to evaluate if the IVST approach is able to maintain a good predicting capability when coolant velocity varies from the training values. The outcomes obtained are reported in Fig. 11, showing the pressure drop of the entire PFU cooling channel and of the ST region only by the test simulations and by the IVST modelling approach, together with 10% error bars. It can be observed that there is a really good agreement between the curves, showing that by adopting this approach it is possible to correctly predict the pressure losses over a broad range of coolant inlet velocities, with relative errors within the 10% range.

4.2. The orthotropic virtual swirl tape approach

The idea behind the definition of a second VST approach, different from the IVST, is to reproduce the pressure drop of the ST region and of the entire PFU cooling channel by adopting a single porous domain with a properly defined momentum sink term, corresponding to the ST region, i.e. the red region in Fig. 8, defined in such a way to produce a swirling motion of the fluid. To obtain this result, the porous medium should be able to determine a preferred direction of fluid motion within its domain, requiring the definition of a non-isotropic momentum source term in the Navier–Stokes equations. According to the rotating slug flow model proposed by Gambill [15], the tangential velocity component u_θ inside a pipe equipped with a ST can be related to the axial velocity u_z by the relation given in Eq. (5), where r is the radial coordinate of the cylindrical coordinate system aligned with the axis of the cooling channel.

$$u_\theta = u_z \frac{\pi r}{H} \tag{5}$$

From this equation, it is possible to calculate the preferred flow direction angle θ with respect to the axial direction, given in Eq. (6), which is a function of r.

$$\theta = \arctan\left(\frac{\pi r}{H}\right) \tag{6}$$

It is then possible to determine the directional cosines of this preferred direction of the fluid $\underline{n}_1$, referred to the local cylindrical coordinate system, as reported in Eq. (7), where the three components are given respectively along the radial, tangential, and axial directions.

$$\underline{n}_1(r) = \begin{bmatrix} 0 \\ \frac{\frac{\pi r}{H}}{\sqrt{1+\left(\frac{\pi r}{H}\right)^2}} \\ \frac{1}{\sqrt{1+\left(\frac{\pi r}{H}\right)^2}} \end{bmatrix} \tag{7}$$

Similarly, the other two orthogonal directions can be defined according to Eq. (8). For clarity, the local coordinate system is depicted in Fig. 12, together with the definition of the angle θ and an indication of the cylindrical coordinate system $\left(\underline{r}, \underline{\varphi}, \underline{z}\right)$ of the single PFU cooling channel.

$$\underline{n}_2(r) = \begin{bmatrix} 0 \\ \frac{-1}{\sqrt{1+\left(\frac{\pi r}{H}\right)^2}} \\ \frac{\frac{\pi r}{H}}{\sqrt{1+\left(\frac{\pi r}{H}\right)^2}} \end{bmatrix}, \underline{n}_3 = \begin{bmatrix} 1 \\ 0 \\ 0 \end{bmatrix} \tag{8}$$

A simple implementation of a numerical model relying on a single porous medium can be based on the adoption of an orthotropic sink term, in which two values of K_{loss} coefficients are given, one (lower) both in the preferred $\underline{n}_1$ and in the radial $\underline{n}_3$ directions, namely $K_{loss,1}$, and another (higher), namely $K_{loss,2}$, along $\underline{n}_2$. This latter can be interpreted as a direction perpendicular to the ST. By adopting a uniform value of $K_{loss,1}$, it is not possible to develop a strong swirling motion, as the fluid is most likely to flow at low values of r, due to the shortest path available. It can be in fact noted that the angle θ is zero at the channel axis line, thus the fluid can move in a straight line, while at high r values, the fluid path is much longer. To compensate for this effect, $K_{loss,1}(r)$ can be defined as a decreasing function with r. The functional form of $K_{loss,1}$ can be chosen arbitrarily, and different formulations have been tested. For the sake of brevity, only the formulation of Eq. (9) is discussed here, where B, C, and R_{crit} are proper parameters, to be defined by means of the optimization procedure.

$$K_{loss,1} = \begin{cases} B & \text{if } r < R_{crit} \\ C/r^2 & \text{if } r \geq R_{crit} \end{cases} \tag{9}$$

It should be noted that R_{crit} can be interpreted as a threshold radius value, necessary to reproduce the blockage effect of the ST in the central part of the cooling channel. Concerning $K_{loss,2}$, a finite high value has to be selected to obtain a compromise between the numerical stability of the simulation and the blockage of fluid motion along the direction perpendicular to the tape. The resulting source term to be adopted in the Navier–Stokes equations is thus defined according to Eq. (10). As it may be noted, the loss coefficient matrix is diagonal, hence the name orthotropic VST.

$$\underline{S} = -\begin{bmatrix} K_{loss,1}(r) & 0 & 0 \\ 0 & K_{loss,2} & 0 \\ 0 & 0 & K_{loss,1}(r) \end{bmatrix} \cdot \underline{u} \frac{\rho}{2} \|\underline{u}\| \tag{10}$$

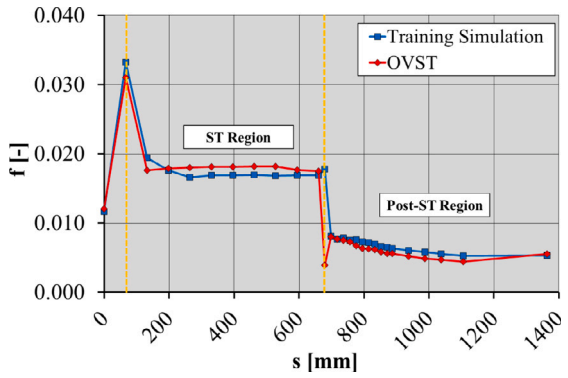

Fig. 13. Comparison of local Fanning friction factor along the PFU cooling channel curvilinear abscissa between training simulation and OVST approach.

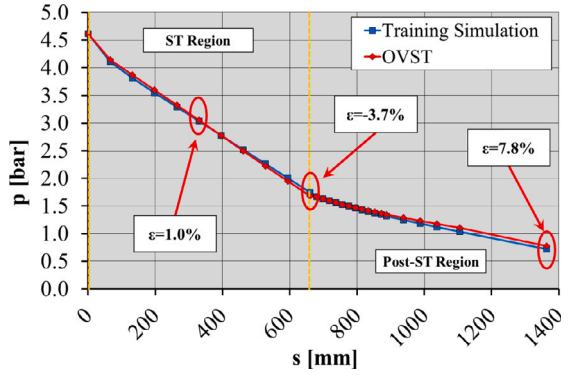

Fig. 14. Comparison of pressure evolution along the PFU cooling channel curvilinear abscissa between training simulation and OVST approach.

The calibration of the OVST has been performed starting from the same training simulation already considered for the IVST, and adopting the same mesh features and simulation settings. The optimization study required ≈ 150 iterations to converge and the comparison between the OVST approach and the training simulation is depicted in Fig. 13 in terms of Fanning friction factor profile and in Fig. 14 in terms of pressure profile, together with an indication of the relative errors.

As shown in Fig. 13, the model can capture the initial peak of the Fanning friction factor, while the pressure drop along the ST region is slightly overestimated. Regarding the post-ST region, the pressure loss is underestimated with respect to the original profile, but the shape of the curve is similar to the training simulation. As visible from Fig. 14, the errors are higher than those reported in Fig. 10, being slightly lower than 8% in the estimation of the outlet pressure. The performance is however acceptable, as the pressure is correctly reproduced along the ST region. Moreover, the error in the prediction of the total pressure drop is ≈ 1.2%.

The resulting flow field is depicted in Fig. 15, showing the fluid swirling motion induced by the OVST porous medium with a detail of the ST section inlet.

It can be observed that no flow separation can be generated since there is no ST solid wall inside the cooling channel. Therefore, the initial peak visible in Fig. 13 is related to the fluid momentum that forces the coolant to move along the pipe axial direction, despite the higher resistance induced by $K_{loss,2}$.

Finally, the OVST approach has been compared with the test simulations, as depicted in Fig. 16. As it can be observed, the pressure drop prediction is good also at velocities different from the training value, with deviations lower than 10%.

Compared to the IVST approach, the friction factor and pressure profile curves are reproduced more precisely, while the global pressure

Fig. 15. Details of the swirling motion induced by the OVST inside the PFU cooling channel.

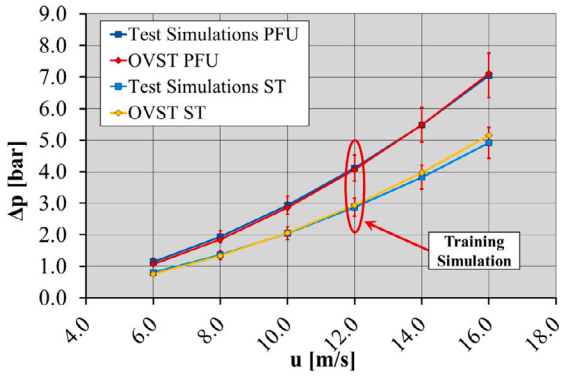

Fig. 16. Comparison of pressure drop prediction between test simulations and OVST approach.

predictions are less accurate but still acceptable. Moreover, differently from the simpler IVST formulation, the mathematical complexity of OVST is significantly higher. Concerning the pre-processing phase of the simulation, the adoption of the OVST approach may be time-consuming, since each PFU cooling channel requires a local cylindrical reference system to be defined. To overcome this limitation, a script has been developed in the SpaceClaim–Python language [16] to automatically calculate the directions of the PFU cooling channels and their centres to properly define the OVSTs porous media.

4.3. Heat transfer prediction capabilities of the virtual swirl tape approaches

Finally, in this latter section, it will be briefly discussed the heat transfer prediction potential of the two VST approaches. The analyses presented here should be intended as preliminary, as they have been performed considering the VST coefficients obtained by an optimization performed only on pressure drop.

A reference PFU cooling channel analysis has been performed, by adopting the same computational mesh of Fig. 4 and the settings of Table 3, to obtain the reference convective heat transfer coefficients h.

The analysis has been performed not considering the solid regions of the PFU assemblies and by assuming a total thermal power of 40 kW, being close to the thermal loads expected for this component

Table 3
Summary of PFU cooling channel hot CFD analysis setup.

Analysis type	Steady-state thermal
Material Library	Water IAPWS IF97 [17]
Turbulence Model	k-ω SST
Boundary Layer Modelling	Automatic wall function
Pipe/ST Roughness	1 μm/0.5 μm
Inlet velocity/temperature	12 m/s / 130 °C
Outlet static pressure	45 bar
ST/Post-ST surface loads	32 kW/8 kW

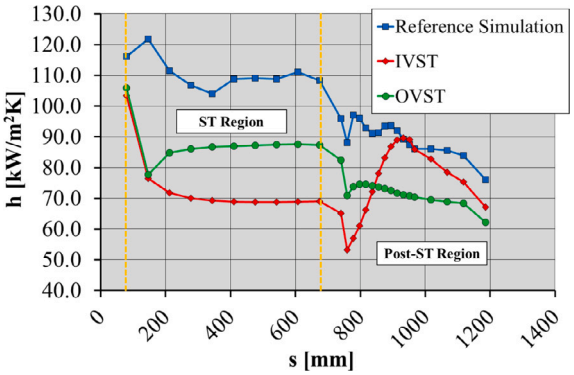

Fig. 17. Comparison of heat transfer coefficient along the PFU cooling channel curvilinear abscissa with the different VST approaches.

for the single-circuit cooling option of [8]. The surface loads have been supposed to be uniform and the breakdown of 32 to 8 kW, respectively for the ST and post-ST regions, has been considered. These values have been obtained from the surface power profiles on the OVT PFUs reported in [18], and have to be intended just as a rough indication to provide an order of magnitude to the thermal loads. In fact, a more realistic assessment should take into account the non-uniformities of the heat flux both along the curvilinear abscissa and around the pipe circumference.

The two VSTs approaches have been then tested under the same conditions of Table 3 and the results obtained are depicted in Fig. 17. As can be argued from the results, the heat transfer prediction capabilities of the VST approaches are not satisfactory. Concerning the IVST, h is underestimated on average by 34% in the ST region and by 16% in the post-ST region, but higher deviations are observed locally. Moreover, the heat transfer coefficient profile is significantly different, especially in the post-ST region. Regarding the OVST, the results are slightly better both in terms of relative error, being equal to 21% in the ST region and 20% in the post-ST region, and curve shape. As can be observed in Fig. 17, the model is able to capture the decaying trend of the heat transfer coefficient in the region downstream of the ST, even if the predicted h values are lower than those of the reference simulation along the entire curvilinear abscissa.

The importance of correctly simulating the heat transfer coefficient of the PFU cooling channels inside the complex divertor geometry is limited, as it is not possible to include all the details of the PFUs in the current CFD calculations. However, in the future will be further studied the possibility of improving the prediction capability of the heat transfer coefficient by finding different functional forms for the loss coefficients adopted by the model, and considering the information on h to calibrate the porous media.

5. Conclusions

A novel simulation technique based on an equivalent porous medium concept, namely the VST approach, has been developed to reduce the computational cost and the pre-processing efforts required to perform CFD simulations of ST-equipped components while maintaining good accuracy in the prediction of the pressure distribution. These porous media are calibrated by selecting optimal parameters by means of dedicated optimization studies, performed with the well-established CFD code ANSYS CFX, coupled with the ANSYS Direct Optimization tool. Two variants of the VST approach have been presented: the IVST and the OVST. The IVST technique is rather simple and is able to capture the global values of pressure drop, losing some details of the pressure profile. The OVST approach is more complex, being able to produce the swirling motion inside the cooling channel, and it is able to capture the pressure profile along the cooling channel with good fidelity. Additionally, the VST thermal performance has been tested in view of their application for coupled thermal simulations. The results obtained are still unsatisfactory, requiring further development, in particular by looking at different loss coefficient functional forms and including heat transfer coefficient information during the calibration phase. However, both IVST and OVST can provide very good results in terms of pressure drop prediction and, therefore, they can be a valuable asset for the simulation of ST-equipped cooling channels in complex CFD simulations.

CRediT authorship contribution statement

A. Quartararo: Conceptualization, Investigation, Methodology, Software, Validation, Visualization, Writing – original draft, Writing – review & editing. **S. Basile:** Supervision, Writing – review & editing, Conceptualization. **G. Bongiovì:** Supervision, Writing – review & editing, Conceptualization. **R. Burlon:** Supervision, Writing – review & editing, Conceptualization. **F.M. Castrovinci:** Investigation, Validation, Visualization, Writing – review & editing, Conceptualization. **I. Catanzaro:** Conceptualization, Writing – review & editing, Supervision. **P. Chiovaro:** Conceptualization, Supervision, Writing – review & editing. **P.A. Di Maio:** Funding acquisition, Project administration, Supervision, Writing – review & editing, Conceptualization. **G. Mazzone:** Funding acquisition, Project administration, Supervision, Writing – review & editing, Conceptualization. **E. Vallone:** Conceptualization, Writing – review & editing, Supervision. **J.H. You:** Funding acquisition, Project administration, Writing – review & editing, Conceptualization.

Declaration of competing interest

The authors declare that they have no known competing financial interests or personal relationships that could have appeared to influence the work reported in this paper.

Data availability

Data will be made available on request.

Acknowledgments

This work has been carried out within the framework of the EUROfusion Consortium, funded by the European Union via the Euratom Research and Training Programme (Grant Agreement No. 101052200 — EUROfusion). Views and opinions expressed are however those of the author(s) only and do not necessarily reflect those of the European Union or the European Commission. Neither the European Union nor the European Commission can be held responsible for them.

References

[1] T. Donné, W. Morris, European Research Roadmap to the Realisation of Fusion Energy, 2018, ISBN: 978-3-00-061152-0.
[2] J.H. You, et al., Divertor of the European DEMO: Engineering and technologies for power exhaust, Fusion Eng. Des. 175 (2022) 113010, http://dx.doi.org/10.1016/j.fusengdes.2022.113010.
[3] A.R. Raffray, et al., Critical heat flux analysis and R&D for the design of the ITER divertor, Fusion Eng. Des. 45 (4) (1999) 377–407, http://dx.doi.org/10.1016/S0920-3796(99)00053-8.

[4] G. Maddaluno, et al., The DTT device: Divertor solutions for alternative configurations including liquid metals, Fusion Eng. Des. 122 (2017) 341–348, http://dx.doi.org/10.1016/j.fusengdes.2017.03.172.
[5] S. Kwon, K. Im, J.S. Park, Thermohydraulic assessment for the modified concept of the K-DEMO divertor target, Fusion Sci. Technol. 72 (4) (2017) 737–746, http://dx.doi.org/10.1080/15361055.2017.1350479.
[6] X.Y. Qian, et al., New designs of target and cooling scheme for water cooled divertor in DEMO, Nucl. Fusion 61 (3) (2021) 036008, http://dx.doi.org/10.1088/1741-4326/abd148.
[7] A. Tincani, et al., Hydraulic characterization of the full scale mock-up of the DEMO divertor outer vertical target, Energies 14 (23) (2021) http://dx.doi.org/10.3390/en14238086.
[8] A. Quartararo, et al., Thermofluid-dynamic assessment of the EU-DEMO divertor single-circuit cooling option, Fusion Eng. Des. 188 (2023) 113408, http://dx.doi.org/10.1016/j.fusengdes.2022.113408.
[9] ANSYS Inc., ANSYS CFX-Solver Theory Guide, 2021, Release: 2021 R1.
[10] ANSYS Inc., ANSYS DesignXplorer User's Guide, 2021, Release: 2021 R1.
[11] D. Marzullo, V. Imbriani, F. Giovanna, DIV-DEMO.S.1-T001-D001_DEMO Divertor CAD Model 2021, 2021, EUROfusion IDM Ref.: 2PHRQZ v1.0.
[12] P.A. Di Maio, et al., Hydraulic assessment of an upgraded pipework arrangement for the DEMO divertor plasma facing components cooling circuit, Fusion Eng. Des. 168 (2021) 112368, http://dx.doi.org/10.1016/j.fusengdes.2021.112368.
[13] R.M. Manglik, A.E. Bergles, Swirl flow heat transfer and pressure drop with twisted-tape inserts, in: J.P. Hartnett, T.F. Irvine, Y.I. Cho, G.A. Greene (Eds.), in: Advances in Heat Transfer, vol. 36, 2003, pp. 183–266, http://dx.doi.org/10.1016/S0065-2717(02)80007-7.
[14] S.E. Haaland, Simple and explicit formulas for the friction factor in turbulent pipe flow, J. Fluids Eng. 105 (1) (1983) 89–90, http://dx.doi.org/10.1115/1.3240948.
[15] W.R. Gambill, Heat Transfer, Burnout, and Pressure Drop for Water in Swirl Flow Through Tubes with Internal Twisted Tapes, vol. 2911, Oak Ridge National Laboratory, 1960.
[16] ANSYS Inc., Discovery SpaceClaim, ANSYS, Canonsburg, PA, USA, 2021, 2021, Release: 2021 R1.
[17] International Association for the Properties of Water and Steam, Revised Release on the IAPWS Industrial Formulation 1997 for the Thermodynamic Properties of Water and Steam, 2007.
[18] E. Vallone, et al., Conference paper. Thermal-hydraulic study of the primary heat transfer system of EU-DEMO divertor plasma facing components, in: The 19th International Topical Meeting on Nuclear Reactor Thermal Hydraulics, NURETH-19. Brussels, Belgium, March 6 - 11, 2022, ISBN 9789076971261, 2022.